



Facile synthesis of RGD peptide-modified iron oxide nanoparticles with ultrahigh relaxivity for targeted MR imaging of tumors

Journal:	<i>Biomaterials Science</i>
Manuscript ID:	BM-ART-01-2015-000037.R1
Article Type:	Paper
Date Submitted by the Author:	24-Feb-2015
Complete List of Authors:	Hu, Yong; Donghua University, Li, Jingchao; Donghua University, Yang, Jia; Shanghai Jiaotong University, Department of Radiology, Shanghai First People's Hospital, School of Medicine Wei, Ping; Donghua University, Luo, Yu; Donghua University, Ding, Ling; Donghua University, Sun, Wenjie; Donghua University, Zhang, Guixiang; Shanghai Jiaotong University, Shi, Xiangyang; Donghua University, College of Chemistry, Chemical Engineering, and Biotechnology Shen, Mingwu; Donghua University,

Cite this: DOI: 10.1039/c0xx00000x

www.rsc.org/xxxxxx

PAPER

Facile synthesis of RGD peptide-modified iron oxide nanoparticles with ultrahigh relaxivity for targeted MR imaging of tumors

Yong Hu^{al}, Jingchao Li^{al}, Jia Yang^{bl}, Ping Wei^a, Yu Luo^a, Ling Ding^a, Wenjie Sun^a, Guixiang Zhang^{b*}, Xiangyang Shi^{a*}, Mingwu Shen^{a*}

5

Received (in XXX, XXX) Xth XXXXXXXXX 20XX, Accepted Xth XXXXXXXXX 20XX

DOI: 10.1039/b000000x

We report the facile synthesis of arginine-glycine-aspartic acid (RGD) peptide-targeted iron oxide (Fe₃O₄) nanoparticles (NPs) with ultrahigh relaxivity for *in vivo* tumor magnetic resonance (MR) imaging. In this study, stable polyethyleneimine (PEI)-coated Fe₃O₄ NPs were first prepared by a mild reduction route. The formed aminated Fe₃O₄ NPs with PEI coating were sequentially conjugated with fluorescein isothiocyanate (FI) and polyethylene glycol (PEG)-RGD segment, followed by acetylation of the remaining PEI surface amines. The thus formed Fe₃O₄@PEI.NHAc-FI-PEG-RGD NPs were characterized *via* different techniques. We show that the multifunctional RGD-targeted Fe₃O₄ NPs with a mean size of 9.1 nm are water-dispersible, colloidal stable, and hemocompatible and cytocompatible in the given concentration range. With the displayed ultrahigh r₂ relaxivity (550.04 mM⁻¹s⁻¹) and RGD-mediated targeting specificity to α_vβ₃ integrin-overexpressing cancer cells as confirmed by flow cytometry and confocal microscopy, the developed multifunctional Fe₃O₄@PEI.NHAc-FI-PEG-RGD NPs are able to be used as a highly efficient nanoprobe for targeted MR imaging of α_vβ₃ integrin-overexpressing cancer cells *in vitro* and the xenografted tumor model *in vivo*. Given the versatile PEI amine-enabled conjugation chemistry, the developed PEI-coated Fe₃O₄ NPs may be functionalized with other biological ligands or drugs for various biomedical applications, in particular diagnosis and therapy of different types of cancer.

Introduction

Magnetic iron oxide (Fe₃O₄) nanoparticles (NPs) have attracted considerable interest in different biomedical applications including but not limited to drug and gene delivery,¹⁻³ biomedical imaging,⁴⁻¹⁰ and hyperthermia.¹¹⁻¹³ In particular, Fe₃O₄ NPs have been used as contrast agents for magnetic resonance (MR) imaging because they can shorten the T₂ relaxation time of water protons, thus resulting in enhanced imaging contrast and sensitivity.^{10, 14, 15} A variety of approaches have been adopted to synthesize Fe₃O₄ NPs for T₂-weighted MR imaging applications such as thermal decomposition,^{16, 17} controlled co-precipitation,^{7, 18-21} and hydrothermal synthesis.^{6, 22-25}

For effective biomedical applications, it is important to render the Fe₃O₄ NPs with good colloidal stability through appropriate surface modification. This is because naked Fe₃O₄ NPs are prone to aggregate due to their large surface energy and strong inherent magnetic dipole interaction.²⁶⁻²⁸ Likewise, the Fe₃O₄ NPs should have reactive surface groups, thus having an ability to be further functionalized to have improved biocompatibility, and to have targeting specificity for MR imaging of different biological systems. For instance, Fe₃O₄ NPs can be silanized to render the particles with amine groups, thereby having good colloidal stability and the ability to be further functionalized.^{6, 17, 29} In our

previous work,²² we have shown that stable polyethyleneimine (PEI)-coated Fe₃O₄ NPs can be successfully synthesized *via* a facile hydrothermal approach. The formed PEI-coated Fe₃O₄ NPs can be modified with polyethylene glycol (PEG) to have improved cytocompatibility and significantly reduced macrophage cellular uptake,²² and be modified with targeting ligand folic acid (FA)⁵ or hyaluronic acid (HA)⁴ for targeted MR imaging of FA receptor- or CD44 receptor-overexpressing cancer cells *in vitro* and *in vivo*, respectively. These studies highlight the importance to prepare Fe₃O₄ NPs with reactive surface functional groups for biomedical imaging applications.

Although the Fe₃O₄ NPs synthesized using the hydrothermal approach reported in our previous work can be used for targeted tumor MR imaging,^{4, 5} the r₂ relaxivity of the Fe₃O₄ NPs is all smaller than 160 mM⁻¹s⁻¹. For highly sensitive T₂-weighted MR imaging applications, it is always desirable to synthesize Fe₃O₄ NPs with improved r₂ relaxivity. Recently, Yao and coworkers reported a mild reduction route to synthesize Fe₃O₄ NPs that can be enveloped by poly(methylacrylic acid) *via* photochemical *in situ* polymerization.³⁰ Due to the different nature of the synthesis method, we attempted to modify the surface of Fe₃O₄ NPs formed *via* the mild reduction method for biomedical applications. For targeted tumor MR imaging, Fe₃O₄ NPs have been modified with various ligands such as arginine-glycine-aspartic acid (RGD)

peptide,¹⁶ antibodies,³¹ folic acid (FA),^{5, 19, 20, 32} hyaluronic acid (HA),^{4, 33} and chlorotoxin.³⁴⁻³⁶ Among these ligands, RGD peptide is quite attractive because it can mediate effective targeting of tumor microvasculature and cancer cells such as glioblastomas³⁷⁻⁴¹ through binding of the overexpressed $\alpha_v\beta_3$ integrin on the cell surface. The prior successes in the synthesis and modification of PEI-coated Fe_3O_4 NPs^{4, 5, 22} lead us to hypothesize that PEI-coated Fe_3O_4 NPs may also be synthesized using a mild reduction route and be functionalized with RGD peptide for targeted MR imaging of $\alpha_v\beta_3$ integrin-overexpressing cancer cells *in vitro* and *in vivo*.

In this present study, we utilized a mild reduction method to produce water-dispersible PEI-coated Fe_3O_4 NPs ($\text{Fe}_3\text{O}_4@\text{PEI.NH}_2$ NPs) that were sequentially conjugated with fluorescein isothiocyanate (FI) and PEGylated RGD (PEG-RGD), followed by acetylation of the remaining PEI surface amines (Scheme 1). The thus formed multifunctional RGD-targeted Fe_3O_4 ($\text{Fe}_3\text{O}_4@\text{PEI.NHAc-FI-PEG-RGD}$) NPs were characterized *via* different techniques. To our surprise, the RGD-targeted Fe_3O_4 NPs displayed ultrahigh relaxivity (up to $550 \text{ mM}^{-1} \text{ s}^{-1}$, see below). Their cytotoxicity and hemocompatibility were evaluated by cell viability assay, cell morphology observation, and hemolysis assay. The RGD-mediated targeting specificity of the particles to $\alpha_v\beta_3$ integrin-overexpressing cancer cells, U87MG cells (a human glioma cell line) was confirmed by flow cytometric analysis and confocal microscopic observation. Furthermore, the developed RGD-targeted Fe_3O_4 NPs were used as a nanoprobe for targeted MR imaging of U87MG cells *in vitro* and the xenografted U87MG tumor model *in vivo*. To our knowledge, this is the first report related to the development of RGD-targeted Fe_3O_4 NPs with ultrahigh relaxivity for tumor MR imaging applications.

Experimental section

Materials

PEG with one end of carboxyl group and the other end of amine group ($\text{NH}_2\text{-PEG-COOH}$, Mw = 2 000) and PEG monomethyl ether with the other end of carboxyl group ($m\text{PEG-COOH}$, Mw = 2 000) were supplied by Shanghai Yanyi Biotechnology Corporation (Shanghai, China). Thiolated cyclic RGD peptide (Mw = 690.93) was purchased from GenicBio (Shanghai, China). N-Succinimidyl 6-maleimidohexanoate (6-M), 1-ethyl-3-[3-dimethylaminopropyl] carbodiimide hydrochloride (EDC), FI, and N-hydroxysuccinimide (NHS) were from J&K Chemical Ltd. (Shanghai, China). Ferric chloride hexahydrate ($\text{FeCl}_3 \cdot 6\text{H}_2\text{O}$) > 99%, branched PEI (Mw = 25 000), ammonia (25%), sodium sulfite, dimethyl sulfoxide (DMSO), triethylamine, acetic anhydride, and all the other chemicals and solvents were acquired from Aldrich (St. Louis, MO). 3-(4,5-Dimethylthiazol-2-yl)-2,5-diphenyltetrazolium bromide (MTT) was purchased from Shanghai Sangon Biological Engineering Technology & Services Co., Ltd (Shanghai, China). U87MG cells were from Institute of Biochemistry and Cell Biology, the Chinese Academy of Sciences (Shanghai, China). Fetal bovine serum (FBS), Dulbecco's modified Eagle's medium (DMEM), penicillin, and streptomycin were obtained from Hangzhou Jinuo Biomedical Technology (Hangzhou, China). Water used in all experiments

with a resistivity higher than $18.2 \text{ M}\Omega\text{-cm}$ was purified by a Milli-Q Plus 185 water purification system (Millipore, Bedford, MA).

60 Preparation of PEI-coated Fe_3O_4 NPs

PEI-coated Fe_3O_4 NPs ($\text{Fe}_3\text{O}_4@\text{PEI.NH}_2$) were synthesized *via* a mild reduction route³⁰ in the presence of PEI. In brief, $\text{FeCl}_3 \cdot 6\text{H}_2\text{O}$ (1.3 g) dissolved in 20 mL water was placed into a 250-mL three-necked flask. The solution was bubbled with nitrogen atmosphere for 15 min under stirring. Then an aqueous sodium sulfite solution (0.2 g, 10 mL) was dropwise added into the above solution under stirring. After 30 min, an aqueous PEI solution (0.5 g, 5 mL) and 2 mL of ammonia was sequentially added into the above mixture solution. Thereafter, the mixture solution was vigorously stirred for 30 min at $60\text{--}70^\circ\text{C}$. After that, the reaction mixture was cooled down to room temperature and stirred for another 1.5 h. The formed $\text{Fe}_3\text{O}_4@\text{PEI.NH}_2$ product was magnetically collected and washed several times with water. Finally, the $\text{Fe}_3\text{O}_4@\text{PEI.NH}_2$ product was centrifuged (8 000 rpm, 10 min) to remove the larger particles, and the supernatant suspension was collected and stored at 4°C before use. For comparison, naked Fe_3O_4 NPs without coating of PEI were also prepared under similar experimental conditions.

Synthesis of $\text{Fe}_3\text{O}_4@\text{PEI.NH}_2\text{-FI}$ NPs

The obtained $\text{Fe}_3\text{O}_4@\text{PEI.NH}_2$ NPs (154 mg) dispersed in water were collected and washed with DMSO for 3 times by virtue of an external magnet, and then re-dispersed in DMSO (10 mL). Then, FI (3.59 mg) dissolved in 1 mL DMSO was dropwise added into the DMSO solution of the $\text{Fe}_3\text{O}_4@\text{PEI.NH}_2$ NPs under vibration in the dark at room temperature. After 24 h, the formed $\text{Fe}_3\text{O}_4@\text{PEI.NH}_2\text{-FI}$ NPs were magnetically collected, purified with DMSO *via* 3 cycles of magnetic separation/washing/redispersion, and finally re-dispersed in 10 mL DMSO.

90 Synthesis of RGD-PEG-COOH

RGD-PEG-COOH was synthesized according to our previous work.⁴⁰ In brief, 6-M (0.012 mmol, 3.70 mg) was first reacted with $\text{NH}_2\text{-PEG-COOH}$ (0.01 mmol, 20 mg) in DMSO (5 mL) at room temperature for 8 h. Then the DMSO solution of RGD (0.01 mmol, 6.91 mg, 2 mL) was dropwise added into the above mixture under vigorous magnetic stirring at room temperature for 12 h. The reaction mixture was then dialyzed against phosphate buffered saline (PBS, 3 times, 2 L) for 1 day and water (3 times, 2 L) for 2 days using a dialysis membrane with molecular weight cut-off (MWCO) of 1 000, followed by lyophilization to obtain the product of RGD-PEG-COOH.

Synthesis of multifunctional RGD-targeted Fe_3O_4 NPs

RGD-PEG-COOH (8.338 mmol, 25 mg), EDC (83.411 mmol, 15.99 mg), and NHS (83.413 mmol, 9.60 mg) were dissolved in 2 mL DMSO, respectively. Then all the three solutions were mixed and stirred for 3 h to activate the carboxyl group of RGD-PEG-COOH. The activated RGD-PEG-COOH was dropwise added into the above DMSO solution of $\text{Fe}_3\text{O}_4@\text{PEI.NH}_2\text{-FI}$ NPs (10 mL) under stirring for 3 days.

The formed $\text{Fe}_3\text{O}_4@\text{PEI.NH}_2\text{-FI-PEG-RGD}$ were collected and washed with DMSO for 1 time and water for 3 times to remove

excess reactants *via* magnetic separation, and dispersed in 10 mL water. The remaining PEI amines on the surface of the formed $\text{Fe}_3\text{O}_4@\text{PEI.NH}_2\text{-FI-PEG-RGD}$ NPs were further acetylated according to our previous reports.^{42, 43} Briefly, triethylamine (505 μL) was first dropwise added into the $\text{Fe}_3\text{O}_4@\text{PEI.NH}_2\text{-FI-PEG-RGD}$ aqueous suspension (10 mL) and the solution was well mixed *via* shaking for 30 min. Then, acetic anhydride (412 μL) was dropwise added into the $\text{Fe}_3\text{O}_4@\text{PEI.NH}_2\text{-FI-PEG-RGD}$ /triethylamine mixture solution under vigorous shaking in the dark for another 24 h. Finally, the product was purified *via* 3 cycles of magnetic separation/washing/redispersion in water. The formed $\text{Fe}_3\text{O}_4@\text{PEI.NHAc-FI-PEG-RGD}$ NPs were dispersed in water (10 mL) and stored at 4 °C for further use. For comparison, non-targeted Fe_3O_4 NPs without RGD conjugation ($\text{Fe}_3\text{O}_4@\text{PEI.NHAc-FI-mPEG}$ NPs) were also prepared in a manner similar to that used to form the $\text{Fe}_3\text{O}_4@\text{PEI.NHAc-FI-PEG-RGD}$ NPs. The only difference is the use of *m*PEG-COOH instead of the use of RGD-PEG-COOH.

Characterization techniques

¹H NMR spectra were collected using a Bruker AV400 nuclear magnetic resonance spectrometer. Samples were dissolved in deuterated DMSO (DMSO-d_6) before measurements. UV-Vis spectroscopy was undertaken using a Lambda 25 UV-Vis spectrophotometer (PerkinElmer, Boston, MA), and samples were dispersed in water before measurements. Zeta potential and dynamic light scattering (DLS) measurements were performed using a Malvern Zetasizer Nano ZS model ZEN3600 (Worcestershire, UK) equipped with a standard 633 nm laser. Samples were dispersed in water at a concentration of 0.1 mg/mL before measurements. Thermal gravimetric analysis (TGA) was performed at a heating rate of 20 °C/min to quantify the composition of samples using a TG 209 F1 (NETZSCH Instruments Co., Ltd., Germany) thermogravimetric analyzer operating in a temperature range of 25-700 °C under flowing nitrogen atmosphere. Transmission electron microscopy (TEM, JEOL 2010F analytical electron microscope, Tokyo, Japan) was carried out to characterize the size and morphology of the NPs at an accelerating voltage of 200 kV. TEM samples were prepared by depositing a dilute particle suspension (5 μL) onto a carbon-coated copper grid and air dried before measurements. For each sample, more than 300 NPs in different TEM images were randomly selected and measured using an ImageJ software to assess the average size and size distribution of the NPs. Leeman Prodigy inductively coupled plasma-optical emission spectroscopy (ICP-OES, Hudson, NH) was used to measure the Fe concentration of the NP suspension. T_2 relaxometry was performed using a 0.5 T NMI20-Analyst NMR Analyzing system (Shanghai Niumag Corporation, Shanghai, China). Samples were diluted in water with Fe concentration in a range of 0.003-0.048 mM before measurements. The instrumental parameters were set as follows: point resolution = 156 mm \times 156 mm, section thickness = 0.6 mm, TR = 4000 ms, TE = 60 ms, and number of excitation = 1. The T_2 relaxivity (r_2) was calculated by linear fitting of $1/T_2$ (s^{-1}) as a function of Fe concentration (mM).

Hemolysis assay

Fresh human blood stabilized with ethylenediaminetetraacetic acid (EDTA) was obtained by Shanghai First People's Hospital

(Shanghai, China) and used after approval by the Shanghai First People's Hospital Ethical Committee. The human red blood cells (HRBCs) were purified according to our previous work.^{44, 45} Then, the suspension of HRBCs was 10 times diluted with PBS. The diluted HRBC suspension (0.1 mL) was added into 0.9 mL water as a positive control, 0.9 mL PBS as a negative control, and 0.9 mL PBS containing RGD-targeted Fe_3O_4 NPs or non-targeted Fe_3O_4 NPs at different Fe concentrations (0.5-8.0 mM), respectively. The mixtures were gently vortexed and then kept still for 2 h at room temperature. After centrifugation at 10 000 rpm for 1 min, the photos of the samples were taken and the absorbance of the supernatants (hemoglobin) was recorded by a Perkin Elmer Lambda 25 UV-Vis spectrophotometer. The hemolysis percentages of different samples were calculated according to a previously reported method.^{6, 18, 43}

Cytotoxicity assay and cell morphology observation

U87MG cells overexpressing $\alpha_v\beta_3$ integrin were routinely cultured and passaged in 25- cm^2 plates in regular DMEM supplemented with 10% heat-inactivated FBS, penicillin (100 U/mL), and streptomycin (100 $\mu\text{g}/\text{mL}$) in a 37 °C incubator with 5% CO_2 .

In vitro cytotoxicity of the RGD-targeted Fe_3O_4 NPs and non-targeted Fe_3O_4 NPs were evaluated by MTT viability assay of U87MG cells. Briefly, 1×10^4 U87MG cells were seeded with 200 μL of DMEM per well into a 96-well plate and cultured at 37 °C and 5% CO_2 overnight to bring the cells to confluence. Then the medium was replaced with 200 μL fresh medium containing PBS (control), RGD-targeted Fe_3O_4 NPs or non-targeted Fe_3O_4 NPs at different Fe concentrations (10, 25, 50, 75, and 100 $\mu\text{g}/\text{mL}$, respectively). After incubation at 37 °C and 5% CO_2 for 24 h, MTT (20 μL in PBS, 5 mg/mL) was added to each well and the cells were incubated under the same culture conditions for an additional 4 h. After that, DMSO (150 μL) was added to replace the culture medium and to dissolve the insoluble formazan crystals. The assays were carried out according to the manufacturer's instructions and the absorbance of each well was recorded using a Thermo Scientific Multiskan MK3 ELISA reader (Thermo scientific, Hudson, NH) at 570 nm. Mean and standard deviation (SD) of 5 parallel wells for each sample were reported. To further confirm the cytotoxicity of the RGD-targeted and non-targeted Fe_3O_4 NPs, the morphology of U87MG cells treated with the NPs at different Fe concentrations (10, 25, 50, 75, and 100 $\mu\text{g}/\text{mL}$, respectively) for 24 h was also observed by phase contrast microscopy (Leica DM IL LED inverted phase contrast microscope) with a magnification of 200 \times for each sample.

Flow cytometry

U87MG cells were seeded in 12-well plates at a density of 2×10^5 cells per well in 1 mL of DMEM and incubated at 37 °C and 5% CO_2 overnight to bring the cells to confluence. Then the medium was replaced with 1 mL fresh medium containing PBS, RGD-targeted Fe_3O_4 NPs or non-targeted Fe_3O_4 NPs at different Fe concentrations (0.125, 0.25, 0.50, 1.00, and 1.50 mM, respectively). After 4 h incubation at 37 °C and 5% CO_2 , the cells were washed 3 times with PBS, trypsinized, centrifugated, and resuspended in 1 mL PBS before flow cytometry analysis using a FACSCalibur flow cytometer (Becton-Dickinson, Franklin

Lakes, NJ). The FL1-fluorescence of 10 000 cells was measured and the measurement of each sample was repeated for 3 times. For comparison, U87MG cells were first incubated with free RGD (2 μ M) for 1 h to block the overexpression of $\alpha_v\beta_3$ integrin. The free RGD-blocked U87MG cells were also treated with the RGD-targeted Fe₃O₄ NPs at different Fe concentrations and analyzed under similar experimental conditions.

Confocal microscopy

Confocal microscopy (Carl Zeiss LSM 700, Jena, Germany) was carried out to confirm the RGD-mediated specific cellular uptake of the multifunctional Fe₃O₄ NPs. In brief, cover slips were first treated and fixed in a 12-well tissue culture plate according to our previous report.⁴ U87MG cells were then seeded into the culture plate at a density of 2×10^5 cells/well with 1 mL fresh medium and cultured at 37 °C and 5% CO₂ overnight to leave the cells well attached onto the cover slips. Then, the medium was replaced with 1 mL fresh medium containing PBS (control), RGD-targeted Fe₃O₄ NPs or non-targeted Fe₃O₄ NPs at an Fe concentration of 0.5 mM. After incubation at 37 °C and 5% CO₂ for 4 h, the cells were rinsed with PBS for 3 times, fixed with glutaraldehyde (2.5%) for 15 min at 4 °C, and counterstained with Hoechst 33342 (1 mg/mL) for 15 min at 37 °C using a standard procedure. The cells on the coverslips were imaged using a 63 \times oil-immersion objective lens. U87MG cells blocked with free RGD (2 μ M) for 1 h were also imaged in a similar manner for comparison.

In vitro MR imaging of cancer cells

U87MG cells were seeded into a 6-well plate at a density of 3×10^6 cells per well with 2 mL DMEM and incubated at 37 °C and 5% CO₂ overnight to bring the cells to confluence. Then the medium was replaced with 2 mL fresh medium containing PBS (control), RGD-targeted Fe₃O₄ NPs, or non-targeted Fe₃O₄ NPs at different Fe concentrations (0.1, 0.2, 0.3, and 0.4 mM, respectively). After incubated at 37 °C and 5% CO₂ for another 6 h, the cells were rinsed with PBS for 5 times, trypsinized, centrifuged, and resuspended in 1 mL PBS (containing 0.5% agarose) in 2-mL Eppendorf tubes before MR imaging. T₂-weighted MR imaging of the cell suspensions was performed by a 3.0 T Signa HDxt superconductor clinical MR system (GE Medical Systems, Milwaukee, WI) with 2 mm slice thickness, 2000/101.2 ms TR/TE, 6 \times 6 cm FOV, and 256 \times 320 matrix.

In vivo MR imaging of a xenografted tumor model

Animal experiments were carried out according to protocols approved by the institutional committee for animal care, and also in accordance with the policy of the National Ministry of Health. To establish the xenografted tumor model, male 4- to 6-week-old BALB/c nude mice (15-20 g, Shanghai Slac Laboratory Animal Center, Shanghai, China) were subcutaneously injected with 3×10^6 cells/mouse in the right hind legs. When the tumor nodules reached a volume of 0.8-1.6 cm³ at about 3 weeks postinjection, the mice were anesthetized by intraperitoneal injection of pentobarbital sodium (40 mg/kg), and then the RGD-targeted or non-targeted Fe₃O₄ NPs were intravenously injected into the nude mice via the tail vein (600 μ g Fe per mouse, in 0.1 mL PBS). After placing the mice inside a custom-built rodent receiver coil (Chenguang Med Tech, Shanghai, China), MR scanning of the

mice was carried out before and after administration of the RGD-targeted or non-targeted Fe₃O₄ NPs at the time points of 0.5, 1, 2, 4, and 24 h postinjection using a 3.0 T Signa HDxt superconductor clinical MR system under similar conditions to those used for *in vitro* MR imaging of cancer cells.

In vivo biodistribution

To assess the biodistribution of the multifunctional Fe₃O₄ NPs, the above tumor-bearing BALB/c nude mice after MR scanning at 24 h post-injection were euthanized and the major organs including the heart, liver, spleen, lung, kidney and tumor were extracted and weighed. The organs were cut into small pieces and digested by aqua regia (nitric acid/hydrochloric acid, v/v = 1:3) for 2 days before ICP-OES quantification of the Fe element. For comparison, the tumor-bearing mice injected with PBS (0.1 mL) were used as control.

Statistical analysis

One-way ANOVA statistical analysis was performed to evaluate the significance of the experimental data. 0.05 was selected as the significance level, and the data were indicated with (*) for $p < 0.05$, (**) for $p < 0.01$, and (***) for $p < 0.001$, respectively.

Results and discussion

Synthesis and characterization of Fe₃O₄@PEI.NHAc-FI-PEG-RGD NPs

By adopting a mild reduction route reported by Yao and coworkers,³⁰ PEI-coated Fe₃O₄ NPs were synthesized by reduction of Fe³⁺ in the presence of PEI. The PEI-coated Fe₃O₄ NPs (Fe₃O₄@PEI.NH₂ NPs) were then sequentially modified with FI via a thiourea linkage and PEGylated RGD via EDC chemistry, followed by acetylation of the remaining PEI surface amines (Scheme 1). The thus formed multifunctional RGD-targeted Fe₃O₄ NPs were characterized via different techniques.

The modification of FI moiety onto the surface of the Fe₃O₄@PEI.NH₂ NPs was confirmed by UV-Vis spectroscopy (Figure S1, Electronic Supplementary Information, ESI). Apparently, the appearance of a prominent absorption peak at 500 nm suggests the successful conjugation of FI onto the particles, in agreement with our previous work.⁵ In contrast, no significant absorption feature can be seen at the same wavelength for the Fe₃O₄@PEI.NH₂ NPs without FI modification.

To modify RGD onto the surface of the Fe₃O₄@PEI.NH₂ NPs, PEGylated RGD (RGD-PEG-COOH) was firstly synthesized by reacting the heterofunctional NH₂-PEG-COOH with 6-M to render the PEG with maleimide end group for subsequent coupling with thiolated RGD via thiol maleimide coupling.⁴⁰ The formed RGD-PEG-COOH segments were characterized by ¹H NMR spectroscopy (Figure S2, ESI). Through the NMR integration of the RGD-associated aromatic proton peaks at 7.3 and 7.4 ppm and the PEG methylene proton at 3.7 ppm, the average number of RGD conjugated to each PEG was estimated to be 0.5. Next, the formed Fe₃O₄@PEI.NH₂-FI NPs were modified with RGD-PEG-COOH or *m*PEG-COOH through EDC chemistry, and were quantitatively characterized by TGA (Figure 1). Clearly, the Fe₃O₄@PEI.NH₂-FI NPs have a weight loss of 12.4% due to the coating of PEI and the modification with FI. After further modification with RGD-PEG-COOH or *m*PEG-

COOH, the weight losses of $\text{Fe}_3\text{O}_4@\text{PEI.NH}_2\text{-FI-PEG-RGD}$ and $\text{Fe}_3\text{O}_4@\text{PEI.NH}_2\text{-FI-}m\text{PEG}$ NPs were estimated to be 16.4% and 15.7%, respectively. Hence, the RGD-PEG-COOH and *m*PEG-COOH modified onto the surface of the $\text{Fe}_3\text{O}_4@\text{PEI.NH}_2\text{-FI}$ NPs were calculated to be 4.0% and 3.3%, respectively.

Zeta potential and hydrodynamic size of each NP product were measured to confirm each step surface modification (Table 1). Clearly, naked Fe_3O_4 NPs without PEI coating have a relatively large particle size of 537.9 nm, which is due to the lack of PEI stabilization and their surface potential was measured to be -8.3 mV. In contrast to the naked Fe_3O_4 NPs, the PEI coating is able to afford the formed $\text{Fe}_3\text{O}_4@\text{PEI.NH}_2$ NPs with decreased hydrodynamic size (71.6 nm) and with a quite positive surface potential (+64.7 mV). To further render the particles with improved cytocompatibility and non-specific cell membrane binding, it's necessary to neutralize the remaining PEI surface amines on the particle surfaces, similar to our previous work.^{5, 23, 24} The surface potential changes of the particles before and after the acetylation reaction were confirmed by zeta potential measurements. As shown in Table 1, the $\text{Fe}_3\text{O}_4@\text{PEI.NH}_2\text{-FI-PEG-RGD}$ and $\text{Fe}_3\text{O}_4@\text{PEI.NH}_2\text{-FI-}m\text{PEG}$ NPs are quite positively charged with surface potential of +59.2 and +54.1 mV, respectively due to the existence of a large amount of remaining PEI amines on the particle surfaces. After acetylation reaction, the surface potential of the formed $\text{Fe}_3\text{O}_4@\text{PEI.NHAc-FI-PEG-RGD}$ and $\text{Fe}_3\text{O}_4@\text{PEI.NHAc-FI-}m\text{PEG}$ NPs were measured to be +28.3 and +26.4 mV, respectively. The decreased surface potential for both NPs confirmed the success of the acetylation reaction. It should be noted that the positive surface potential of the NPs is not able to be completely neutralized in the presence of excess acetic anhydride. This could be due to that fact that a portion of the PEI amines used to stabilize the Fe_3O_4 NPs cannot be acetylated, in good agreement with our previous reports.^{22, 24}

The hydrodynamic size of the formed NPs was determined by DLS (Table 1). It is clear that the $\text{Fe}_3\text{O}_4@\text{PEI.NH}_2\text{-FI-PEG-RGD}$, $\text{Fe}_3\text{O}_4@\text{PEI.NH}_2\text{-FI-}m\text{PEG}$, $\text{Fe}_3\text{O}_4@\text{PEI.NHAc-FI-PEG-RGD}$ and $\text{Fe}_3\text{O}_4@\text{PEI.NHAc-FI-}m\text{PEG}$ NPs have a hydrodynamic size of 126.2 nm, 108.9 nm, 146.5 nm, and 127.3 nm, respectively. It appears that the acetylation reaction of the remaining PEI surface amines does not appreciably affect their hydrodynamic size. For biomedical applications, the formed targeted and non-targeted NPs should possess a good colloidal stability. The hydrodynamic size of the targeted and non-targeted NPs was occasionally checked by DLS within a time period of 2 weeks (Figure S3, ESI). We show that the hydrodynamic sizes of both NPs do not have appreciable changes, suggesting their good colloidal stability. The colloidal stability of both particles was also assessed by exposing them to water, PBS, and cell culture medium for one month. We show that both NPs are colloidally stable and no precipitation occurs (Figure S3, inset, ESI), further confirming their excellent colloidal stability.

TEM was used to characterize the size and morphology of the formed RGD-targeted Fe_3O_4 NPs (Figure 2a) and non-targeted Fe_3O_4 NPs (Figure 2b). It is clear that most of the particles display a spherical or quasi-spherical shape with a relatively uniform size distribution. The mean diameters of the targeted and non-targeted Fe_3O_4 NPs were measured to be 9.1 ± 1.9 nm and 9.0 ± 1.7 nm, respectively. It is worth noting that the measured

particle size for each NP by TEM is much smaller than that measured by DLS. This can be ascribed to the fact that TEM measures the size of a single particle, while DLS measures the size of particle clusters dispersed in aqueous solution that may consist of many single particles.^{22, 43, 46}

T₂ relaxometry

The transverse relaxation time (T_2) of water protons in an aqueous solution of the formed RGD-targeted and non-targeted Fe_3O_4 NPs was measured at 0.5 T to explore their potential for MR imaging applications. From the T_2 -weighted MR images (Figure 3a), it can be seen that both NPs are able to decrease the MR signal intensity with the increase of Fe concentration. By plotting the relaxation rate ($1/T_2$) as a function of the Fe concentration, the r_2 relaxivity of the RGD-targeted and non-targeted Fe_3O_4 NPs was calculated to be 550.04 and 545.70 $\text{mM}^{-1}\text{s}^{-1}$, respectively (Figure 3b). Interestingly, both NPs display a much higher r_2 value than other Fe_3O_4 NPs prepared by hydrothermal approach or co-precipitation route,^{5, 6, 18, 22} rendering them with an ability for highly sensitive T_2 -weighted MR imaging applications. The exact mechanism related to the ultrahigh r_2 relaxivity is still unclear. It may be due to the nature of the mild synthesis method that can generate particles with extremely high magnetic dipole interaction.

Hemolysis assay

For *in vivo* biomedical applications, the developed nanoprobe should possess good hemocompatibility. The hemocompatibility of the formed RGD-targeted (Figure 4) and non-targeted (Figure S4, ESI) Fe_3O_4 NPs was evaluated by hemolysis assay. Note that the tested Fe concentration in the hemolysis assay should be in line with the *in vivo* MR imaging and biodistribution experiments. According to the literature⁴⁷ and assuming the laboratory mice (20 g) with a blood volume of 2 mL, the Fe concentration in the blood of the injected mice was estimated to be 5.4 mM (600 mg Fe per mouse), which is in the tested Fe concentration range (0.5-8.0 mM). Therefore, we selected the Fe concentration at 0.5-8.0 mM for the hemolysis assay. No obvious hemolysis phenomenon was observed when the HRBCs were exposed to either RGD-targeted or non-targeted Fe_3O_4 NPs at different Fe concentrations (0.5, 1.0, 2.0, 4.0, and 8.0 mM, respectively), similar to the negative PBS control. In contrast, when the HRBCs were exposed to water (positive control), significant hemolysis occurred. The hemolysis percentages of both NPs are less than 5.5% in the studied Fe concentration range (0-8.0 mM), suggesting their negligible hemolytic activity.

Cytotoxicity assay and cell morphology observation

Next, the cytotoxicity of the formed RGD-targeted and non-targeted Fe_3O_4 NPs was evaluated by MTT cell viability assay (Figure 5). It can be seen that the viability of the U87MG cells is higher than 80% after treatment with either RGD-targeted or non-targeted Fe_3O_4 NPs in the given Fe concentration range (0-100 $\mu\text{g/mL}$), suggesting their good cytocompatibility. The cytocompatibility of both NPs were further evaluated by phase contrast microscopic observation of the cells treated with the particles at different Fe concentrations (10, 25, 50, 75, and 100 $\mu\text{g/mL}$) for 24 h (Figure S5, ESI). It is clear that the treated U87MG cells do not display any appreciable morphological

changes when compared with the control cells treated with PBS (Figure S5a and S5g) even at the Fe concentration of 100 $\mu\text{g}/\text{mL}$ (Figure S5f and S5l). The cell morphology observation corroborates the MTT assay data, suggesting that both NPs are non-cytotoxic in the given concentration range.

Flow cytometry assay

To explore the RGD-mediated targeting specificity of the multifunctional Fe_3O_4 NPs, flow cytometry assay of the U87MG cells was performed by virtue of the green fluorescence associated to the attached FI moiety (Figure S6, ESI). Clearly, U87MG cells treated with the non-targeted Fe_3O_4 NPs and free RGD-blocked U87MG cells treated with the RGD-targeted Fe_3O_4 NPs display much lower fluorescence signal intensity than the U87MG cells treated with the RGD-targeted Fe_3O_4 NPs at the same Fe concentrations. This can also be reflected by the quantification of the mean fluorescence of the U87MG cells (Figure 6). The significantly high fluorescence signal intensity of the U87MG cells treated with the RGD-targeted Fe_3O_4 NPs implies that the attached RGD ligands onto the particles are able to mediate the specific targeting of the particles to $\alpha_v\beta_3$ integrin-overexpressing U87MG cells, in agreement with the literature.³⁷⁻⁴⁰ The increased cellular uptake of the non-targeted Fe_3O_4 NPs by U87MG cells and targeted Fe_3O_4 NPs by the free RGD-blocking U87MG cells with the Fe concentration may be ascribed to two different mechanisms: phagocytosis and diffusion *via* cell walls.^{18, 22, 48, 49}

Confocal microscopy

The modification of FI moiety onto the surface of the Fe_3O_4 NPs also enabled confocal microscopic tracking of the intracellular localization of the particles. Figure 7 shows the confocal microscopic images of the U87MG cells treated with PBS, RGD-targeted Fe_3O_4 NPs, or non-targeted Fe_3O_4 NPs at the Fe concentration of 0.5 mM for 4 h, respectively. For comparison, free RGD-blocked U87MG cells were also tested under similar instrumental conditions. Clearly, the free RGD-blocked U87MG cells treated with RGD-targeted Fe_3O_4 NPs (Figure 7b), the U87MG cells treated with the non-targeted Fe_3O_4 NPs (Figure 7c) do not show apparent fluorescence signals, which is similar to the control cells treated with PBS (Figure 7a). In sharp contrast, only the U87MG cells treated with the RGD-targeted Fe_3O_4 NPs display prominent green fluorescent signals in the cytosol and on the cell surfaces, which is associated with the cellular uptake of the particles labeled with the FI moiety (Figure 7d). These results clearly indicate that the specific binding and uptake of the RGD-targeted NPs should be mediated by the $\alpha_v\beta_3$ integrin receptors overexpressed on the cell surfaces, in good agreement with the results of flow cytometry assay.

Targeted MR imaging of cancer cells *in vitro*

With the proven targeting specificity of the RGD-targeted Fe_3O_4 NPs and the ultrahigh r_2 relaxivity, we next explored the potential to use them as a nanoprobe for targeted MR imaging of cancer cells *in vitro*. T_2 -weighted MR images of the U87MG cells treated with either RGD-targeted or non-targeted Fe_3O_4 NPs at different Fe concentrations (0.1, 0.2, 0.3, and 0.4 mM, respectively) were obtained (Figure 8a) and the signal intensity of the cells was quantified (Figure 8b). It is clear that both NPs are

able to decrease the MR signal intensity of the cells with the Fe concentration. However, the decreasing trend of the MR signal intensity of the U87MG cells treated with the RGD-targeted Fe_3O_4 NPs is much more significant. This can be further clearly reflected by quantitative analysis of the MR signal intensity of the cells as a function of Fe concentration (Figure 8b). Apparently, the signal intensity of the U87MG cells treated with the RGD-targeted Fe_3O_4 NPs is much lower than that treated with the non-targeted Fe_3O_4 NPs at each tested Fe concentration ($p < 0.001$). These results suggest that the developed multifunctional Fe_3O_4 NPs can be used as a promising nanoprobe for targeted MR imaging of $\alpha_v\beta_3$ integrin-overexpressing cancer cells *in vitro*.

In vivo MR imaging of U87MG tumor model

We next applied the developed multifunctional Fe_3O_4 NPs as a nanoprobe for targeted MR imaging of a xenografted tumor model *in vivo*. Non-targeted Fe_3O_4 NPs were also used for comparison. The T_2 -weighted MR images of the tumors were colored to allow easy differentiation of the contrast enhancement (Figure 9). From Figure 9a, we can see that the tumor MR signal of all mice gradually decreases with the time postinjection, which is due to the fact that the particles are able to be gradually accumulated into the tumor sites. At 1 h postinjection, both particles are able to induce the weakest tumor MR signal intensity. At 2 h postinjection, the tumor MR signal intensity starts to recover, presumably because the particles have undergone a further metabolism process and a portion of the particles are able to escape from the tumor site. Clearly, the tumor MR signal intensity after treated with the RGD-targeted Fe_3O_4 NPs is much lower than that after treated with the non-targeted Fe_3O_4 NPs at the same time point postinjection of the respective particles. This can be further validated by quantifying the MR signal intensity as a function of the time postinjection of the particles (Figure 9b). The tumor MR signal intensity after injection of the RGD-targeted Fe_3O_4 NPs is significantly lower than that after injection of the non-targeted Fe_3O_4 NPs at 0.5, 1, 2, and 4 h postinjection, respectively ($p < 0.05$). At 24 h postinjection, the tumor MR signal of the mice treated with either RGD-targeted or non-targeted Fe_3O_4 NPs recovers to some extent. Our results suggest that the developed multifunctional Fe_3O_4 NPs are able to be used a nanoprobe for targeted MR imaging of tumors through RGD-mediated targeting pathway.

In vivo biodistribution

For *in vivo* biomedical imaging applications, it's important to understand the biodistribution behavior of the developed multifunctional Fe_3O_4 NPs. ICP-OES was performed to analyze the accumulation of RGD-targeted or non-targeted Fe_3O_4 NPs in several major organs including the heart, liver, spleen, lung, kidney, and tumor at 24 h postinjection (Figure S7, ESI). It is clear that the Fe concentration in the liver, spleen and lung of the mice treated with either non-targeted or RGD-targeted Fe_3O_4 NPs is much higher than that of the control mice treated with PBS. In addition, a smaller amount of uptake can also be found in the heart, kidney and tumor tissue. Our results suggest that both Fe_3O_4 NPs can be excreted from the living body at 24 h postinjection, in agreement with the MR imaging data.

Conclusion

In summary, we developed a facile approach to synthesizing multifunctional RGD peptide-targeted Fe₃O₄ NPs with ultrahigh r₂ relaxivity for MR imaging of tumors. The mild reduction route enabled the synthesis of PEI-coated Fe₃O₄ NPs that can be further conjugated with FI and PEGylated RGD *via* PEI amine-mediated conjugation chemistry. The formed multifunctional Fe₃O₄ NPs possess good water dispersibility, colloidal stability, and cytocompatibility and hemocompatibility in the given Fe concentration range. With the demonstrated ultrahigh r₂ relaxivity (550.04 mM⁻¹s⁻¹) and the RGD-mediated targeting specificity to α_vβ₃ integrin-overexpressing cancer cells, the developed multifunctional RGD-targeted Fe₃O₄ NPs are able to be used as an efficient nanoprobe for targeted MR imaging of α_vβ₃ integrin-overexpressing cancer cells *in vitro* and the xenografted tumor model *in vivo*. Taking into the consideration of the PEI amine-enabled conjugation chemistry, the PEI-coated Fe₃O₄ NPs may be further functionalized with anticancer drugs or other targeting ligands, thereby providing a unique nanoplatform for targeted MR imaging and therapy of different types of cancer.

Acknowledgements

This research is financially supported by the National Natural Science Foundation of China (21273032, 81101150, 81341050, and 81371623), the Sino-German Center for Research Promotion (GZ899), and the Program for Professor of Special Appointment (Eastern Scholar) at Shanghai Institutions of Higher Learning.

Notes and references

^a State Key Laboratory for Modification of Chemical Fibers and Polymer Materials, College of Chemistry, Chemical Engineering and Biotechnology, Donghua University, Shanghai 201620, P. R. China. E-mail: xshi@dhu.edu.cn, mingwu_shen@yahoo.com.

^b Department of Radiology, Shanghai First People's Hospital, School of Medicine, Shanghai Jiaotong University, Shanghai 200080, P. R. China. E-mail: guixiangzhang@sina.com

[†] Authors contributed equally to this work.

† Electronic supplementary information (ESI) available: additional experimental results.

- F. H. Chen, Q. Gao and J. Z. Ni, *Nanotechnology*, 2008, **19**, 165103.
- Y. Zhu, Y. Fang and S. Kaskel, *J. Phys. Chem. C*, 2010, **114**, 16382-16388.
- B. Pan, D. Cui, Y. Sheng, C. Ozkan, F. Gao, R. He, Q. Li, P. Xu and T. Huang, *Cancer Res.*, 2007, **67**, 8156-8163.
- J. Li, Y. He, W. Sun, Y. Luo, H. Cai, Y. Pan, M. Shen, J. Xia and X. Shi, *Biomaterials*, 2014, **35**, 3666-3677.
- J. Li, L. Zheng, H. Cai, W. Sun, M. Shen, G. Zhang and X. Shi, *Biomaterials*, 2013, **34**, 8382-8392.
- M. Shen, H. Cai, X. Wang, X. Cao, K. Li, S. H. Wang, R. Guo, L. Zheng, G. Zhang and X. Shi, *Nanotechnology*, 2012, **23**, 105601.
- X. Shi, T. P. Thomas, L. A. Myc, A. Kotlyar and J. R. Baker Jr, *Phys. Chem. Chem. Phys.*, 2007, **9**, 5712-5720.
- R. Guo and X. Shi, *Curr. Drug Metab.*, 2012, **13**, 1097-1109.
- Y. Hu, J. Li, M. Shen and X. Shi, *Chin. Phys. B*, 2014, **23**, 78704-78711.
- H. Lee, E. Lee, D. K. Kim, N. K. Jang, Y. Y. Jeong and S. Jon, *J. Am. Chem. Soc.*, 2006, **128**, 7383-7389.
- L. Cheng, K. Yang, Y. Li, X. Zeng, M. Shao, S.-T. Lee and Z. Liu, *Biomaterials*, 2012, **33**, 2215-2222.
- Y. Wang, H. Wang, D. Liu, S. Song, X. Wang and H. Zhang, *Biomaterials*, 2013, **34**, 7715-7724.
- X. Ma, H. Tao, K. Yang, L. Feng, L. Cheng, X. Shi, Y. Li, L. Guo and Z. Liu, *Nano Res.*, 2012, **5**, 199-212.
- Y.-M. Huh, Y.-w. Jun, H.-T. Song, S. Kim, J.-s. Choi, J.-H. Lee, S. Yoon, K.-S. Kim, J.-S. Shin and J.-S. Suh, *J. Am. Chem. Soc.*, 2005, **127**, 12387-12391.
- S. Mohapatra, S. K. Mallick, T. K. Maiti, S. K. Ghosh and P. Pramanik, *Nanotechnology*, 2007, **18**, 385102.
- J. Xie, K. Chen, H.-Y. Lee, C. Xu, A. R. Hsu, S. Peng, X. Chen and S. Sun, *J. Am. Chem. Soc.*, 2008, **130**, 7542-7543.
- H. Yang, Y. Zhuang, Y. Sun, A. Dai, X. Shi, D. Wu, F. Li, H. Hu and S. Yang, *Biomaterials*, 2011, **32**, 4584-4593.
- H. Cai, K. Li, M. Shen, S. Wen, Y. Luo, C. Peng, G. Zhang and X. Shi, *J. Mater. Chem.*, 2012, **22**, 15110-15120.
- X. Shi, S. H. Wang, S. D. Swanson, S. Ge, Z. Cao, M. E. Van Antwerp, K. J. Landmark and J. R. Baker, *Adv. Mater.*, 2008, **20**, 1671-1678.
- S. H. Wang, X. Shi, M. Van Antwerp, Z. Cao, S. D. Swanson, X. Bi and J. R. Baker, *Adv. Funct. Mater.*, 2007, **17**, 3043-3050.
- Z. Qiao and X. Shi, *Prog. Polym. Sci.*, 2014, DOI: 10.1016/j.progpolymsci.2014.1008.1002.
- H. Cai, X. An, J. Cui, J. Li, S. Wen, K. Li, M. Shen, L. Zheng, G. Zhang and X. Shi, *ACS Appl. Mater. Interfaces*, 2013, **5**, 1722-1731.
- J. Li, X. Shi and M. Shen, *Part. Part. Syst. Charact.*, 2014, **31**, 1223-1237.
- J. Li, L. Zheng, H. Cai, W. Sun, M. Shen, G. Zhang and X. Shi, *ACS Appl. Mater. Interfaces*, 2013, **5**, 10357-10366.
- S. Ge, X. Shi, K. Sun, C. Li, C. Uher, J. R. Baker Jr, M. M. Banaszak Holl and B. G. Orr, *J. Phys. Chem. C*, 2009, **113**, 13593-13599.
- D. Liu, J. Shi, L. Tong, X. Ren, Q. Li and H. Yang, *J. Nanopart. Res.*, 2012, **14**, 1-7.
- X. Sun, F. Liu, L. Sun, Q. Wang and Y. Ding, *J. Inorg. Organomet. Polym. Mater.*, 2012, **22**, 311-315.
- M. Bagherzadeh, M. M. Haghdoost, F. M. Moghaddam, B. K. Foroushani, S. Saryazdi and E. Payab, *J. Coord. Chem.*, 2013, **66**, 3025-3036.
- K. Li, M. Shen, L. Zheng, J. Zhao, Q. Quan, X. Shi and G. Zhang, *Nanoscale Res. Lett.*, 2014, **9**, 304.
- J. Hong, D. Xu, J. Yu, P. Gong, H. Ma and S. Yao, *Nanotechnology*, 2007, **18**, 135608.
- C. G. Hadjipanayis, R. Machaidze, M. Kaluzova, L. Wang, A. J. Schuette, H. Chen, X. Wu and H. Mao, *Cancer Res.*, 2010, **70**, 6303-6312.
- C. Sun, R. Sze and M. Zhang, *J. Biomed. Mater. Res. Part A*, 2006, **78**, 550-557.
- Y. Lee, H. Lee, Y. B. Kim, J. Kim, T. Hyeon, H. Park, P. B. Messersmith and T. G. Park, *Adv. Mater.*, 2008, **20**, 4154-4157.
- C. Sun, O. Veiseh, J. Gunn, C. Fang, S. Hansen, D. Lee, R. Sze, R. G. Ellenbogen, J. Olson and M. Zhang, *Small*, 2008, **4**, 372-379.
- O. Veiseh, F. M. Kievit, C. Fang, N. Mu, S. Jana, M. C. Leung, H. Mok, R. G. Ellenbogen, J. O. Park and M. Zhang, *Biomaterials*, 2010, **31**, 8032-8042.

-
36. C. Sun, C. Fang, Z. Stephen, O. Veiseh, S. Hansen, D. Lee, R. G. Ellenbogen, J. Olson and M. Zhang, *Nanomedicine*, 2008, **3**, 495-505.
37. X. Chen, P. S. Conti and R. A. Moats, *Cancer Res.*, 2004, **64**, 8009-8014.
38. L. Zhang, H. Xue, C. Gao, L. Carr, J. Wang, B. Chu and S. Jiang, *Biomaterials*, 2010, **31**, 6582-6588.
39. W. Cai and X. Chen, *Nat. Protoc.*, 2008, **3**, 89-96.
40. X. He, C. Alves, N. Oliveira, J. Rodrigues, J. Zhu, I. Bányai, H. Tomás and X. Shi, *Colloids Surf. B: Biointerfaces*, 2015, **125**, 82-89.
41. R. Shukla, E. Hill, X. Shi, J. Kim, M. C. Muniz, K. Sun and J. R. Baker, *Soft Matter*, 2008, **4**, 2160-2163.
42. C. Peng, H. Wang, R. Guo, M. Shen, X. Cao, M. Zhu, G. Zhang and X. Shi, *J. Appl. Polym. Sci.*, 2011, **119**, 1673-1682.
43. H. Liu, Y. Xu, S. Wen, Q. Chen, L. Zheng, M. Shen, J. Zhao, G. Zhang and X. Shi, *Chem.-Eur. J.*, 2013, **19**, 6409-6416.
44. Y. Zhao, S. Wang, Q. Guo, M. Shen and X. Shi, *J. Appl. Polym. Sci.*, 2013, **127**, 4825-4832.
45. C. Peng, K. Li, X. Cao, T. Xiao, W. Hou, L. Zheng, R. Guo, M. Shen, G. Zhang and X. Shi, *Nanoscale*, 2012, **4**, 6768 - 6778.
46. H. Liu, Y. Xu, S. Wen, J. Zhu, L. Zheng, M. Shen, J. Zhao, G. Zhang and X. Shi, *Polym. Chem.*, 2013, **4**, 1788-1795.
47. A. C. Riches, J. G. Sharp, D. B. Thomas and S. V. Smith, *J. Physiol.*, 1973, **228**, 279-284.
48. H. Wang, L. Zheng, C. Peng, R. Guo, M. Shen, X. Shi and G. Zhang, *Biomaterials*, 2011, **32**, 2979-2988.
49. H. Yang, C. Zhang, X. Shi, H. Hu, X. Du, Y. Fang, Y. Ma, H. Wu and S. Yang, *Biomaterials*, 2010, **31**, 3667-3673.

30

Table 1. Zeta potentials and hydrodynamic sizes of the naked Fe₃O₄, Fe₃O₄@PEI.NH₂, Fe₃O₄@PEI.NH₂-FI-*m*PEG, Fe₃O₄@PEI.NHAc-FI-*m*PEG, Fe₃O₄@PEI.NH₂-FI-PEG-RGD, and Fe₃O₄@PEI.NHAc-FI-PEG-RGD NPs. Data are provided as mean ± SD (n = 3).

Materials	Zeta potential (mV)	Hydrodynamic size (nm)	Polydispersity index (PDI)
Naked Fe ₃ O ₄	-8.3 ± 0.5	537.9 ± 10.7	0.45 ± 0.09
Fe ₃ O ₄ @PEI.NH ₂	64.7 ± 2.0	71.6 ± 0.5	0.14 ± 0.01
Fe ₃ O ₄ @PEI.NH ₂ -FI- <i>m</i> PEG	54.1 ± 1.6	108.9 ± 0.6	0.10 ± 0.02
Fe ₃ O ₄ @PEI.NHAc-FI- <i>m</i> PEG	26.4 ± 1.2	127.3 ± 0.4	0.24 ± 0.01
Fe ₃ O ₄ @PEI.NH ₂ -FI-PEG-RGD	59.2 ± 0.3	126.2 ± 2.2	0.13 ± 0.00
Fe ₃ O ₄ @PEI.NHAc-FI-PEG-RGD	28.3 ± 0.2	146.5 ± 2.4	0.17 ± 0.02

Figure captions

Scheme 1. Schematic representation of the synthesis of RGD-PEG-COOH (a) and the $\text{Fe}_3\text{O}_4@PEI.NHAc-FI-mPEG$ and $\text{Fe}_3\text{O}_4@PEI.NHAc-FI-PEG-RGD$ NPs (b). TEA and Ac_2O represent triethylamine and acetic anhydride, respectively.

Figure 1. TGA curves of the $\text{Fe}_3\text{O}_4@PEI.NH_2-FI$ (Curve 1), $\text{Fe}_3\text{O}_4@PEI.NH_2-FI-mPEG$ (Curve 2), and $\text{Fe}_3\text{O}_4@PEI.NH_2-FI-PEG-RGD$ (Curve 3) NPs.

Figure 2. TEM micrographs and size distribution histograms of the RGD-targeted (a) and non-targeted (b) Fe_3O_4 NPs.

Figure 3. Color T_2 -weighted MR images (a) and linear fitting of $1/T_2$ (b) of the non-targeted and RGD-targeted Fe_3O_4 NPs at an Fe concentration of 0.003, 0.006, 0.012, 0.024, and 0.048 mM, respectively. 1 and 2 represent the non-targeted and RGD-targeted Fe_3O_4 NPs, respectively. The color bar from red to blue indicates the gradual decrease of MR signal intensity.

Figure 4. Hemolytical activity of the RGD-targeted Fe_3O_4 NPs at different Fe concentrations (0.5, 1.0, 2.0, 4.0, and 8.0 mM, respectively). PBS and water were used as negative and positive control, respectively. The bottom-right inset shows the photograph of HRBCs exposed to water, PBS, and PBS containing NPs at different Fe concentrations for 2 h, followed by centrifugation. The upper-right inset shows the enlarged UV-Vis spectra.

Figure 5. MTT viability assay of U87MG cells after treatment with the non-targeted and RGD-targeted Fe_3O_4 NPs in an Fe concentration range of 0-100 $\mu\text{g}/\text{mL}$ for 24 h. U87MG cells treated with PBS were used as control.

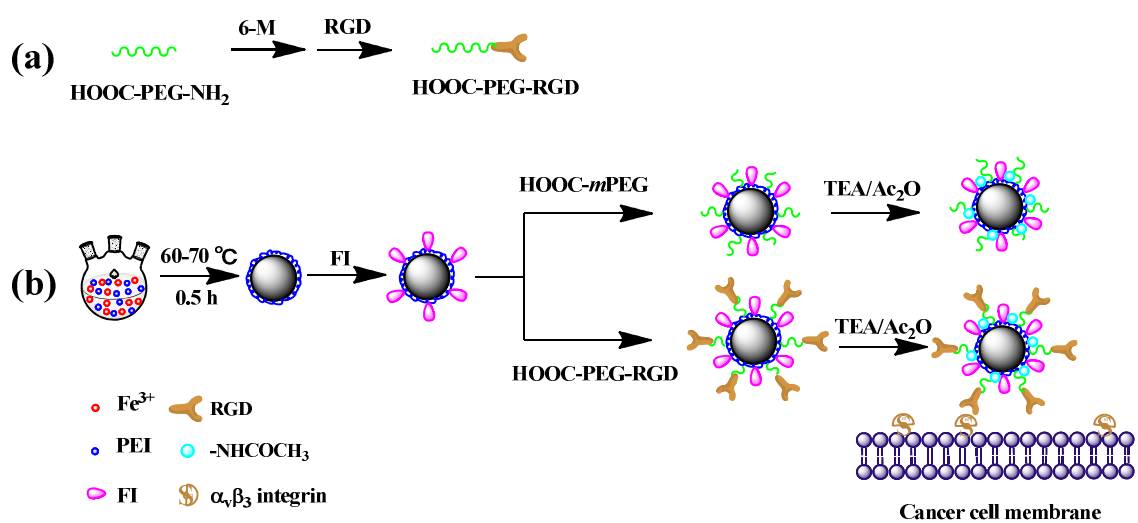
Figure 6. Flow cytometric analysis of the mean fluorescence of the U87MG cells (treated with PBS,

non-targeted Fe₃O₄ NPs, and RGD-targeted Fe₃O₄ NPs, respectively for 4 h) and free RGD-blocked U87MG cells (treated with the RGD-targeted Fe₃O₄ NPs for 4 h) at different Fe concentrations.

Figure 7. Confocal microscopic analysis of the U87MG cells treated with PBS (a), non-targeted Fe₃O₄ NPs (c), and RGD-targeted Fe₃O₄ NPs (d), and free RGD-blocked U87MG cells treated with the RGD-targeted Fe₃O₄ NPs (b). Both cells were treated at an Fe concentration of 0.5 mM for 4 h.

Figure 8. Color T₂-weighted MR imaging (a) and MR signal intensity analysis (b) of U87MG cells treated with PBS, non-targeted Fe₃O₄ NPs, and RGD-targeted Fe₃O₄ NPs at an Fe concentration of 0.1, 0.2, 0.3 and 0.4 mM, respectively for 6 h. The color bar from red to blue indicates the gradual decrease of MR signal intensity. In (a), 1 and 2 represent the non-targeted and RGD-targeted Fe₃O₄ NPs, respectively.

Figure 9. *In vivo* MR imaging (a) and signal intensity analysis (b) of tumors after intravenous injection of the non-targeted and RGD-targeted Fe₃O₄ NPs (600 μg Fe, 0.1 mL PBS for each mouse) at different time points postinjection. Groups 1 and 2 indicate the non-targeted and RGD-targeted Fe₃O₄ NPs, respectively.



Scheme 1

Hu et al.

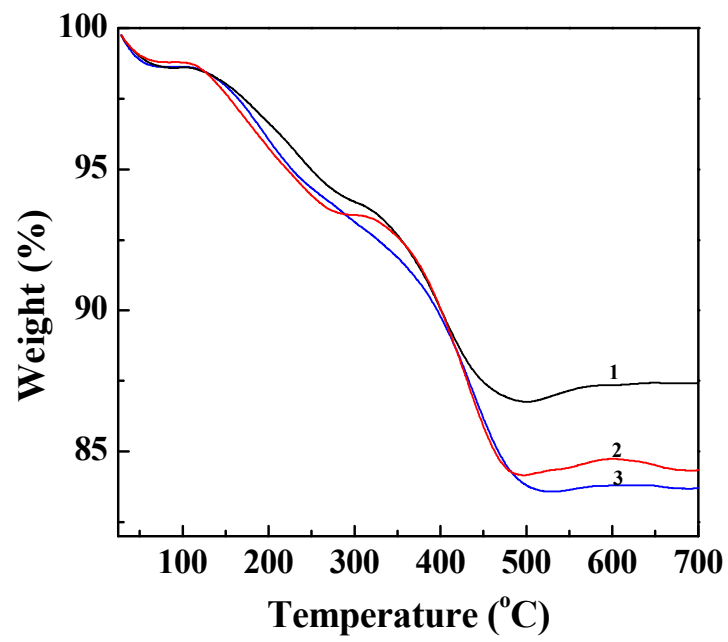


Figure 1

Hu et al.

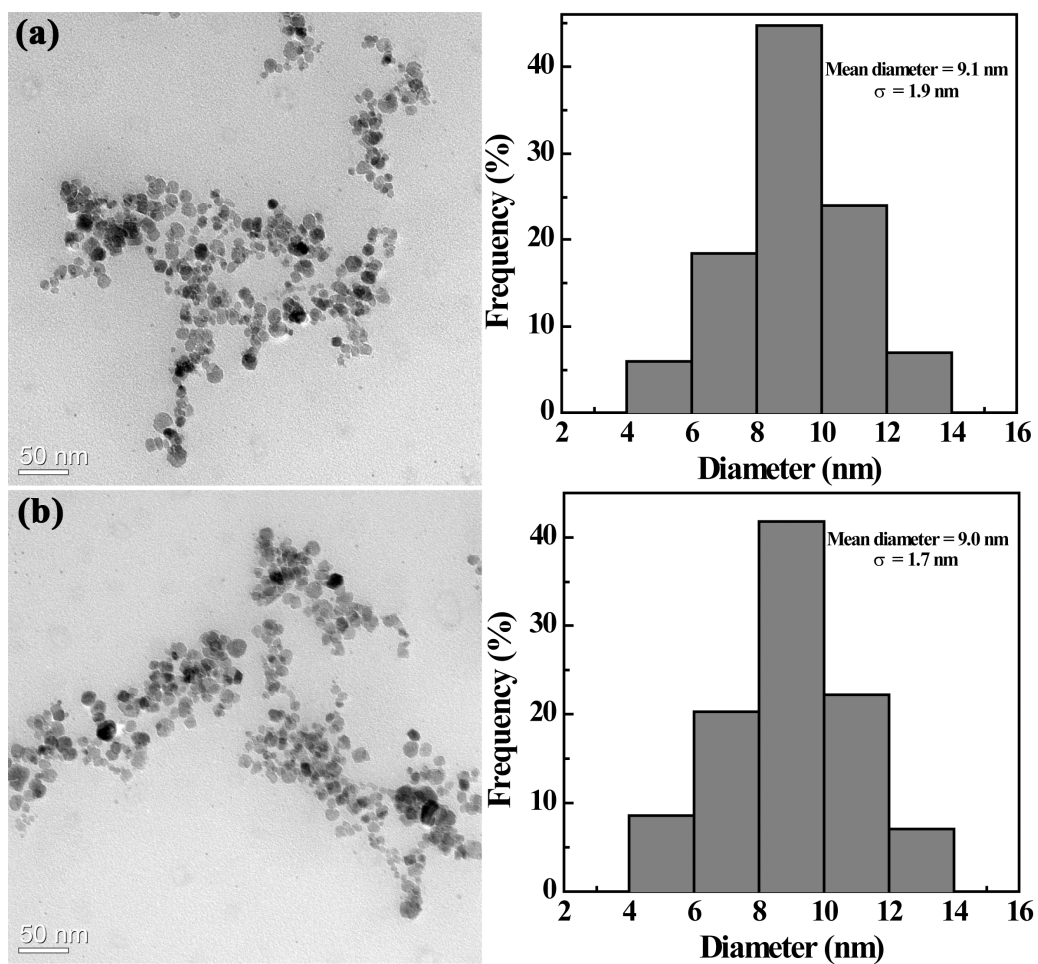


Figure 2

Hu et al.

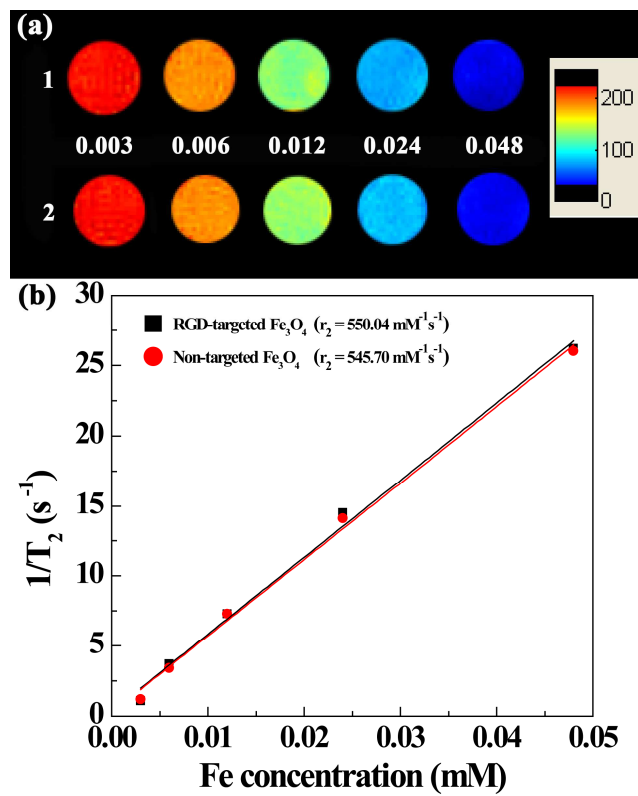


Figure 3

Hu et al.

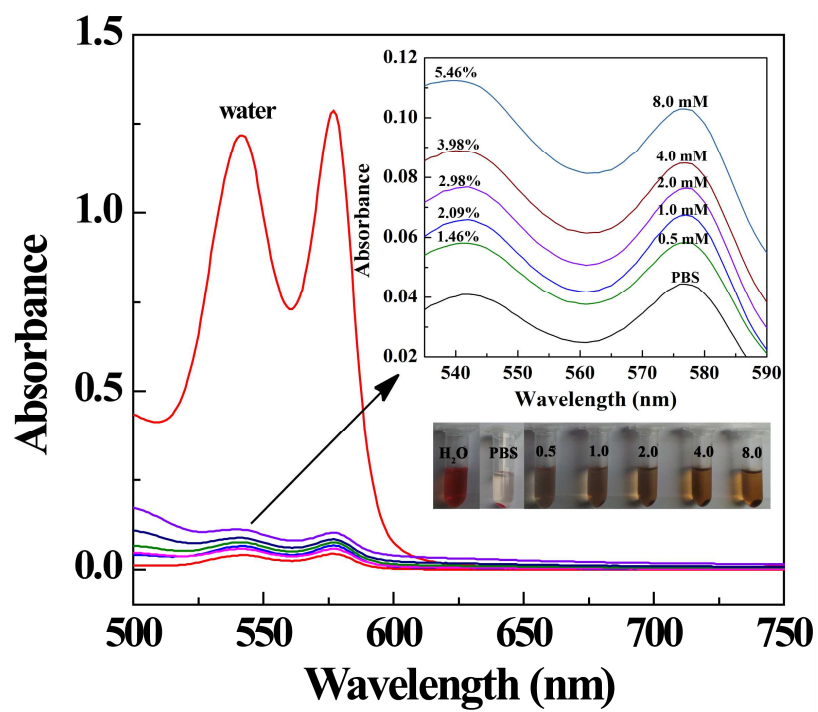


Figure 4
Hu et al.

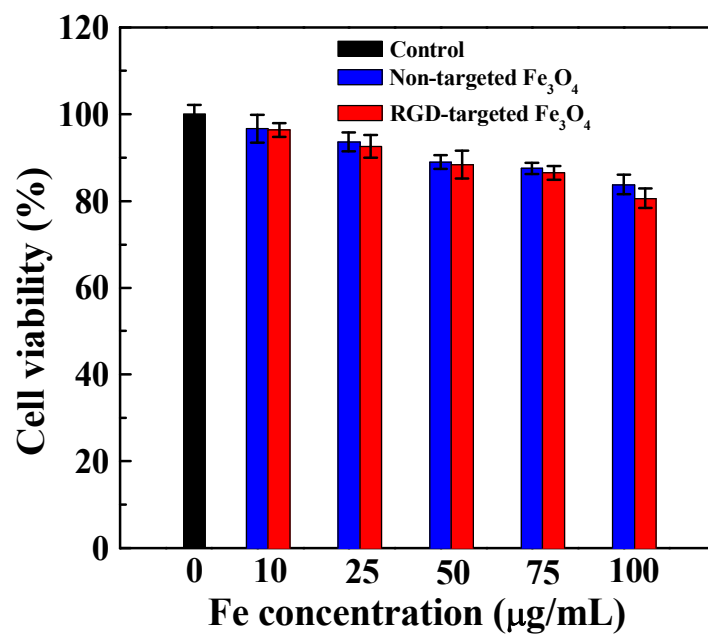


Figure 5

Hu et al.

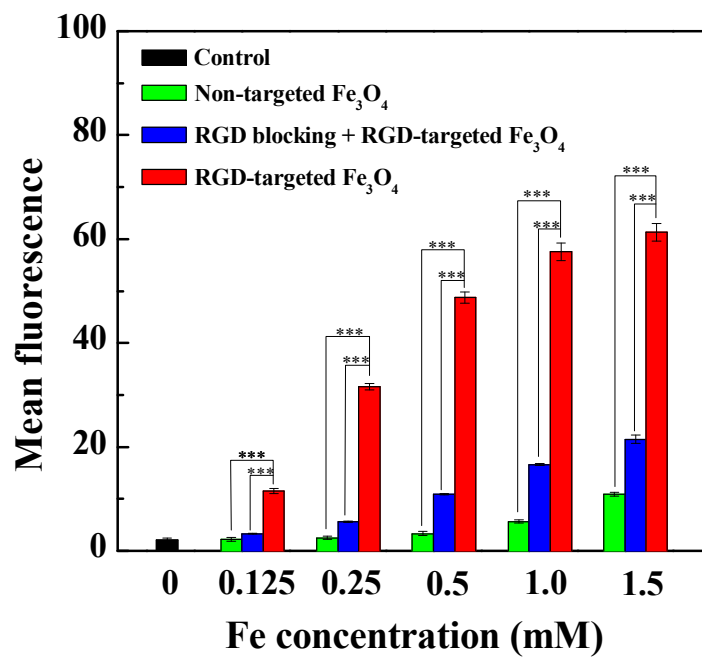


Figure 6

Hu et al.

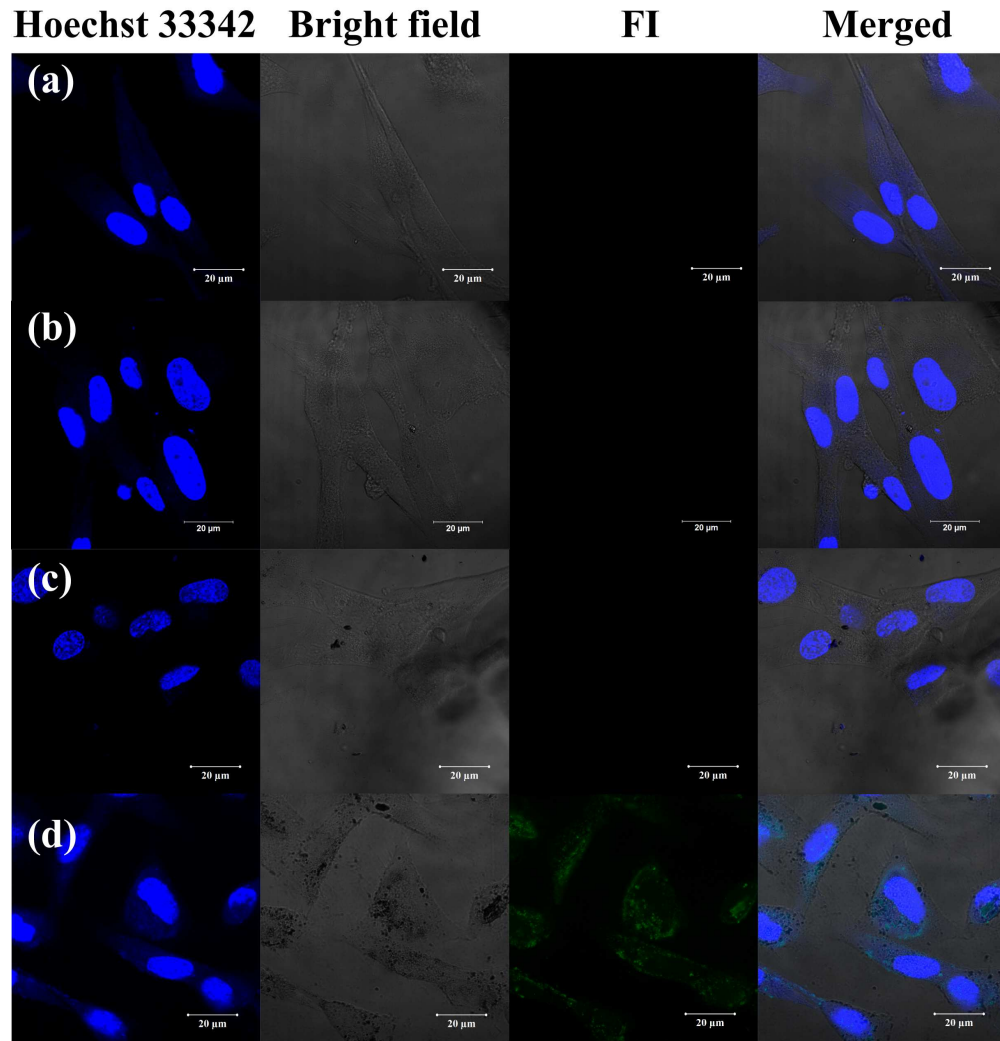


Figure 7

Hu et al.

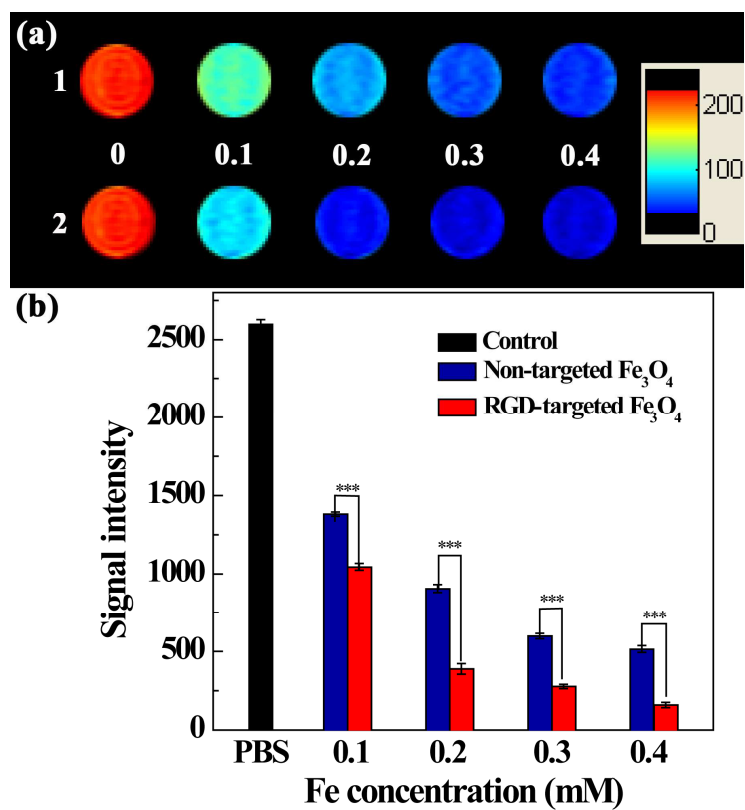


Figure 8

Hu et al.

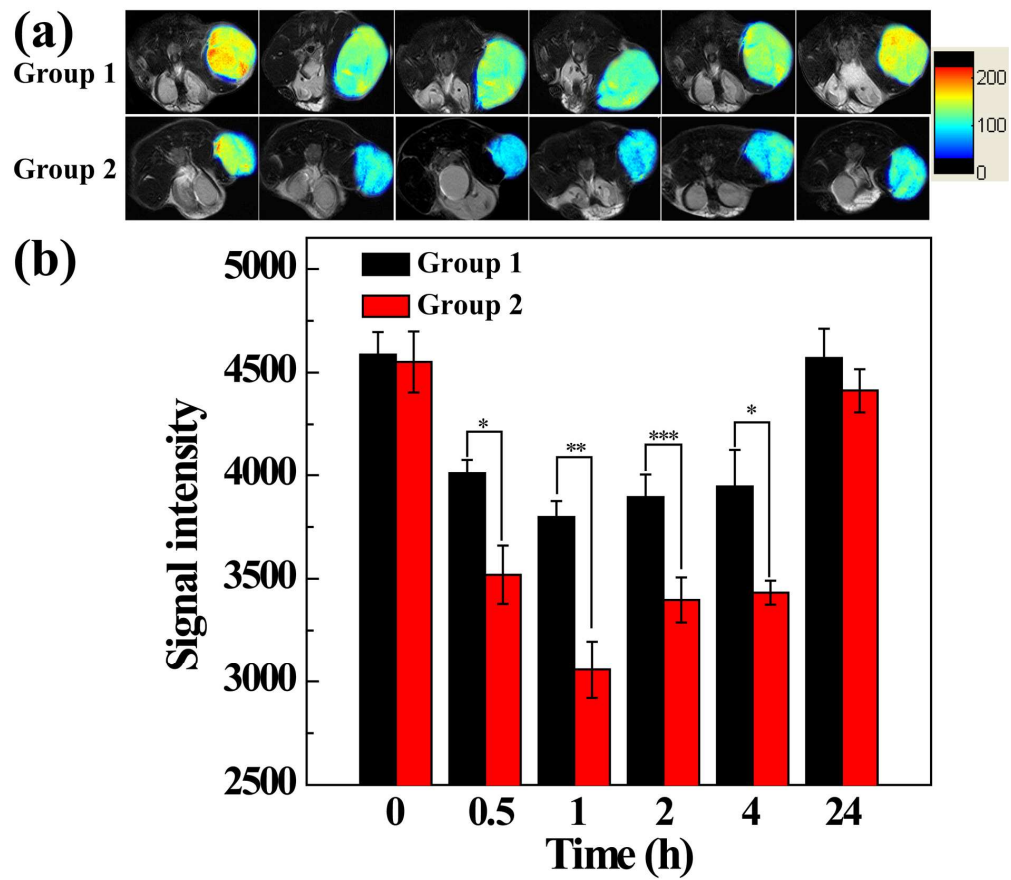


Figure 9

Hu et al.